CHALMERS
UNIVERSITY OF TECHNOLOGY

Interference Analysis and Modeling of Positioning Reference Signals in 5G NTN

Citation for the original published paper (version of record):
Gonzalez-Garrido, A., Querol, J., Wymeersch, H. et al (2024). Interference Analysis and Modeling of Positioning Reference Signals in 5G NTN. IEEE Open Journal of the Communications Society, In Press. http://dx.doi.org/10.1109/OJCOMS.2024.3503692

(article starts on next page)

IEEE Open Journal of the Communications Society

Received XX Month, 2024; revised XX Month, 2024; accepted XX Month, 2024; Date of publication XX Month, 2024; date of current version XX Month, 2024.

Digital Object Identifier 10.1109/TBD

Interference analysis and modeling of Positioning Reference Signals in 5G NTN

Alejandro Gonzalez-Garrido*, ***Student, IEEE***, Jorge Querol*, ***Member, IEEE***, Henk Wymeersch†, ***Fellow, IEEE***, Symeon Chatzinotas*, ***Fellow, IEEE***,

*Interdisciplinary Centre for Security, Reliability and Trust. SnT. University of Luxembourg

†Department of Electrical Engineering, Chalmers University of Technology

Corresponding author: Alejandro Gonzalez-Garrido, email: alejandro.gonzalez@uni.lu

ABSTRACT

The integration of Positioning, Navigation, and Timing (PNT) services within the 5G non-terrestrial networks (NTN) infrastructure is necessary to eliminate the need for a GNSS receiver in the user terminal. Using the positioning reference signal (PRS) in an NTN scenario presents significant challenges, such as interference analysis from the transmission of multiple PRS signals. This study provides a stochastic model for the interference generated by PRS transmissions in a 5G NTN scenario. This model has been derived empirically from a Monte Carlo simulator designed specifically for this purpose, showing that the distribution that best fits the interference is a Generalized Extreme Value (GEV) distribution. The parameters of this distribution are also modeled based on the PRS configuration. Therefore, a designer can use this model to evaluate the probability of encountering certain levels of interference.

INDEX TERMS 5G, NTN, PNT, PRS, interference, SINR, GEV distribution.

I. Introduction

ONE key reason for extending fifth generation (5G) services to non-terrestrial network (NTN) scenarios is the pursuit of global coverage for data and communication services. From Release 17, NTN user equipments (UEs) are mandated to incorporate a global navigation satellite system (GNSS) receiver to access NTN services [1]. However, this requirement poses significant challenges due to the inherent limitations of GNSS receivers in the 5G NTN scenario.

GNSS receivers face limitations such as signal blockage and attenuation, especially in urban environments and dense foliage, as well as multipath effects due to signal reflections off surfaces like buildings and terrain. These issues degrade positioning accuracy and reliability. Additionally, GNSS signals are susceptible to jamming and spoofing attacks, posing security risks in critical applications [2]. The high Doppler shifts caused by the relative motion between satellites and UEs in NTN scenarios complicate signal acquisition and tracking. Furthermore, the power consumption of GNSS receivers in Internet of things (IoT) devices can compromise their commercial viability, especially for battery-powered devices that require a long operational lifetime [3]. These limitations not only affect the reliability and accuracy of positioning but also limit the ability of satellite network operators (SNOs) to offer their services in GNSS-denied areas where line of sight (LOS) with satellites exists, but signals are compromised by jamming or spoofing attacks.

Consequently, developing a GNSS-free UE for NTN operation is critical. This necessity motivates the exploration of providing positioning, navigation, and timing (PNT) services alongside data services through a unified NTN infrastructure. Integrating PNT services within the 5G NTN framework could enhance resilience, improve security, and

This work is licensed under a Creative Commons Attribution 4.0 License. For more information, see https://creativecommons.org/licenses/by/4.0/

provide high-precision, low-latency positioning essential for emerging applications.

In 3rd Generation Partnership Project (3GPP) Release 16 of 5G, positioning features were standardized to offer PNT services [4]. Among various positioning techniques, the use of a specific downlink signal, positioning reference signal (PRS), is notable for its wider bandwidth and higher carrier frequencies compared to previous generations, reaching up to 100 MHz in the frequency region 1 (FR1) band and up to 400 MHz in the frequency region 2 (FR2) band [5], [6]. However, the current definition of 5G PNT services necessitates a network connection for the subscriber; that is, 5G PNT services are on-demand by the UE, the core network, or a third party connected to the core network, in contrast to GNSS, which is a broadcast service. This architecture, inherited from Long Term Evolution (LTE), was initially designed for emergency call requirements as a terrestrial positioning system. In this framework, the network informs the UE about the PRS configuration; subsequently, the UE acquires and relays the measurements back to the core network, which then performs position estimation. This approach poses scalability challenges in terms of the number of simultaneous users and is impractical in NTN scenarios where a network connection may not be established prior to positioning.

Moreover, from Release 17 onward, 5G networks include NTN elements such as unmanned aerial vehicles (UAVs), high-altitude platforms (HAPs), and satellites, increasingly emphasized by industry stakeholders to facilitate global communication capabilities [7]. An NTN feature similar to GNSS is the ephemeris dissemination of satellites via the system information block (SIB)19 message. However, the accuracy required for these ephemerides is not as high as in GNSS since precise positioning is not needed for communication use cases. In an NTN satellite scenario, each UE requires position information prior to its initial access. Therefore, current standardized 5G positioning techniques are impractical in an NTN scenario due to the prerequisite of a network connection for the UE.

Looking beyond 5G, the upcoming 6G network is expected to establish a unified network entity characterized by multiple connectivity layers designed to meet the requirements of various devices in diverse scenarios [8]. The convergence of network PNT services with NTN offers numerous advantages, including the development of an autonomous integrated communication and navigation system under a unified network infrastructure [9]. Recent studies highlight the technological potential to achieve a truly integrated communication, location, and sensing system [10]. Furthermore, the industry is making progress with the development of services such as Xona [11], the ESA LEO-PNT mission [12], and the Geesat constellation from ESA and China. However, these commercial developments do not include a communication service, emphasizing the need for integrated solutions.

In this context, developing GNSS-free PNT services integrated within the 5G NTN infrastructure is essential. Such an approach would mitigate the limitations of GNSS receivers, provide reliable and secure PNT services, and support emerging applications requiring high-precision positioning. This study explores the feasibility and implementation of offering PNT services alongside data services through a unified NTN infrastructure, aiming to contribute to the advancement of integrated communication and navigation systems.

A. State of the Art

Although the integration of communication and navigation systems within a unified network, as highlighted in the previous paragraph, holds the promise of revolutionizing PNT solutions, it also introduces new challenges in signal interference management. The literature on interference in orthogonal frequency-division multiplexing (OFDM) systems, as illustrated by [13]–[15], focuses mainly on terrestrial communication scenarios, addressing inter-symbol interference (ISI) issues in multipath environments. This existing research is pivotal for understanding interference dynamics; however, it primarily explores scenarios involving single transmitters. Furthermore, studies such as [16], [17] delve into inter-numerology interference (INI) modeling and improvement strategies, primarily in single-transmitter scenarios with inter-carrier interference (ICI), ISI, and INI as the main sources of interference.

The complexity increases manifold when considering integrated systems, where multiple transmitters and receivers interact within a shared spectral environment. Similar approaches are already available in the literature for terrestrial networks, such as in [18], where a fraction frequency reuse (FFR) scheme is proposed, or the concept of Network-MIMO, developed in [19] for indoor scenarios. However, none of these are intended for navigation systems. Therefore, advanced interference management techniques must be developed to meet the unique requirements of an integrated communication and navigation system, ensuring the reliability and accuracy essential for such a converged network infrastructure [20]. This gap in existing research underscores the need for comprehensive studies that extend beyond traditional interference models to address the complexities of integrated systems in future networks.

In a satellite scenario, the delays between the signals from different satellites (in the millisecond range) significantly exceed the length of the cyclix prefix (CP) of the waveform (in the microsecond range) [21]. This leads to ISI and ICI at the receiver located in areas where inter-satellite beams overlap. Assuming that all satellites are synchronized and transmit positioning pilots synchronously in the same bandwidth part (BWP), two strategies are considered in the literature to address interference. In the first strategy, the next generation base station (gNB) applies a temporal guard band, called muting [22]. This is used in terrestrial scenarios, as

the maximum delay is shorter than the CP. However, in a satellite scenario, the muting duration must be long enough for the signal to reach each beam edge; for this reason, a muting scheme is not envisioned for NTN scenarios. The second strategy is for satellites to exploit the low probability of signal collision due to the large differential delay between satellites [23].

Despite significant advancements in interference analysis for 5G NTN scenarios, a critical area remains underexplored: the aggregated interference effects caused by positioning signal transmissions, such as the PRS, within an NTN context. Current research does not thoroughly investigate the interference generated by differential propagation delays between satellites, which are considerably longer than the duration of the PRS slot [21]. It is essential for system designers to ensure that interference levels between PRS and data transmissions are minimized, allowing the receiver to accurately decode data symbols and extract positioning observables.

This area of study is crucial for the development and optimization of LEO PNT services. By meticulously characterizing and modeling interference phenomena and understanding their impact on received signals, robust positioning algorithms and techniques can be developed to effectively mitigate interference effects. This will greatly improve the accuracy and reliability of positioning services, addressing the growing demand for precision in contemporary applications.

B. Paper Contributions

In this paper, we model the interference from broadcasting multiple PRS signals among different satellite gNBs in a BWP. We assume the terrestrial multiplexing scheme for multiple PRS signals [24] and adapt it to an NTN scenario.

Our proposal adopts an approach similar to that used by GNSS; in this case, the SNO dedicates a BWP for broadcasting the PRS, termed bandwidth part for positioning (BWPP). Within the BWPP, the network operator broadcasts the PRS from all satellites. This framework requires a comprehensive analysis of the generated interference, ensuring that it remains sufficiently low for the receiver to decode the data symbols accurately. Our study proposes a model of interference in such a system. The main benefit of broadcasting the PRS is that these signals are accessible to all users, similar to GNSS. This approach enables UE to initiate access to the NTN without requiring a GNSS receiver.

The primary objective of this research is to model the maximum interference power received by a user terminal on the ground. The study focuses on the statistical characteristics of interference, which are critical for UE position estimation. In traditional statistical modeling, the primary focus is on the central tendency of the data, with metrics such as the mean, median, variance, and interquartile range typically used to describe the most common observations within a dataset. However, there exists a specialized branch of statistics that concentrates on extreme events, specifically the tails of distributions. Unlike simple outliers, which might be attributed to data entry errors, these extreme values represent genuine occurrences within the data that are significantly distant from the central tendency and, despite their rarity, can have substantial relevance and impact. As a result, in our analysis of interference, these extreme values, which degrade receiver performance, cannot be ignored.

Extreme value statistics provide the tools to model these rare events, allowing for the estimation and prediction of extreme outcomes, much like traditional statistics do for central tendencies. Due to the infrequency of high interference values, a larger number of simulations is often required to perform a robust analysis.

The contributions of this study include the following:

1) Conduct a theoretical analysis of the received signal and the interference generated by the simultaneous reception of four PRS signals at the receiver. This interference is calculated at the output of the matched filter at the receiver.
2) Explore the potential of applying extreme value statistics, specifically the block maxima approach, to characterize wireless signal interference. By focusing on the extreme values of interference, this approach not only provides a novel metric for assessing signal quality but also facilitates the comparison of different waveform configurations under conditions of rare but impactful interference events. This method, adapted from fields where the impact of extreme events is critical, offers valuable insights into the performance and reliability of wireless communication systems.
3) Develop a Monte Carlo simulator to evaluate the interference generated by the PRS. The PRS can be configured for different numbers of symbols, Comb Sizes, and transmitted power. It outputs the delay/Doppler map (DDM) as a matched filter at the receiver for all received signals.
4) Extract a novel stochastic model of the interference generated by the PRS. This model is based on the configuration of the PRS, such as the transmitted power, the number of symbols, and the Comb Size used at the transmitter side. The model fitting is performed empirically using the results from the previously designed Monte Carlo simulator, confirming the extreme value theorem empirically.

The structure of this paper is as follows: Section II details the scenario and the channel model for low Earth orbit (LEO). Section III presents the signal models used in NTN, the matched filter at the receiver, and the interference model. Section IV describes the Monte Carlo simulator developed and the empirical interference model extracted from the simulation results. Finally, Section V discusses the

conclusions drawn from this study and suggests directions for future research.

II. Scenario for 5G Satellite Positioning

This section outlines the framework and scenario definition for PNT service provision via 5G NTN. It involves a detailed examination of the assumptions, simplifications, and the reasoning behind them. The proposed model requires that the signal from at least four distinct NTN gNBs, similar to GNSS, reaches the user terminal.

In GNSS systems, all satellites carry on board a very precise atomic clock. These clocks are used to keep them synchronized, and the user is notified of any deviation through the navigation message. In our particular scenario, we assume that all satellites are perfectly synchronized, as solving this challenge is beyond the scope of this paper. An initial approach is presented by Prol et al. in [25].

In our study, we adopt an Earth-moving beam configuration, where the satellite beam moves along with the satellite, as defined in 3GPP TR 38.821, without loss of generality, as the interference will be analyzed for single snapshot estimations. For multibeam satellites, the satellite implements precompensation at a reference ground point for each beam, effectively reducing the maximum delay/Doppler range experienced by the signal. Consequently, a single-beam satellite represents a worst-case scenario from this perspective, which we focus on in our analysis.

Nowadays, beam overlapping can be achieved by massive constellations such as Starlink (in our case, we assume a single shell where all satellites are at the same altitude). There are examples in the literature, such as [26], on how to achieve this beam overlapping for a data service.

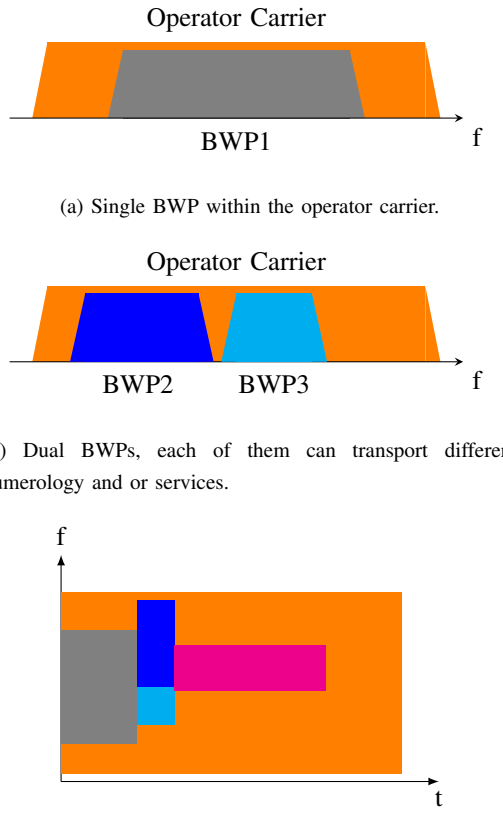

(a) Single BWP within the operator carrier.

(b) Dual BWPs, each of them can transport different numerology and or services.

(c) Dynamic allocation of BWP depending on the resource needs.

Fig. 1: Split of operator spectrum in different BWP in frequency and time.

A. Frequency reuse in a common 5G Resource Grid

In a positioning system, the UE must receive several signals to extract the observables. In the case of a 3D position using time of arrival (ToA), the UE must receive the PRS from at least four satellites to estimate its state, including position and clock bias, $[x, y, z, \delta]$. A multiplexing scheme must be devised to address the simultaneous reception of four signals, taking into account the high delays and Doppler shift characteristics of the NTN channel. This multiplexing scheme must ensure that the user can receive all four signals with minimal aggregate interference. In this regard, a 5G network operator can dynamically allocate its physical resources (time and frequency) based on the requirements of the use case. This dynamic allocation is referred to by 3GPP as BWP, wherein the signals for different user profiles are partitioned in frequency or time, depending on the resources requested or available, as illustrated in Figure 1.

In this study, we implement the PRS multiplexing design used for terrestrial applications [24], as depicted in Figure 2. This design facilitates the transmission of multiple PRS signals within a single OFDM slot, whereby the empty resource elements (REs) left by one transmitter, due to the steps of the subcarrier (”Comb Size” parameter), are used by another gNB for its PRS allocation.

Unlike the terrestrial channel, the NTN channel experiences larger differential delays and Doppler shifts. Our analysis focuses on the interference generated by different transmissions in this scenario, where each satellite’s signal travels through a wireless channel that can be assumed to be independent and uncorrelated for each satellite. A challenge in this scenario is modeling the maximum interference between transmissions from different satellites.

B. Satellite Scenario

The initial step in evaluating a satellite system involves determining the service requirements, which, in turn, establishes a minimum signal to interference plus noise ratio (SINR) at the perimeter of the service beam. Achieving this required SINR primarily depends on mitigating the link loss, with the key factor being the distance between the satellite and the user at the edge of the beam, denoted as ρ_{MAX}

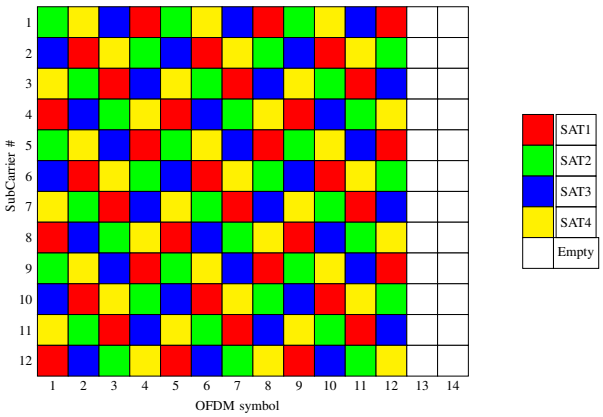

Fig. 2: 5G PRS Transmitted Resource Grid example to multiplex 4 different satellites (each color is the PRS transmission from a different satellite). Size 1 Resource Block $\times$ 1 Slot and a Comb Size (frequency periodicity of the PRS per transmitter) of 4.

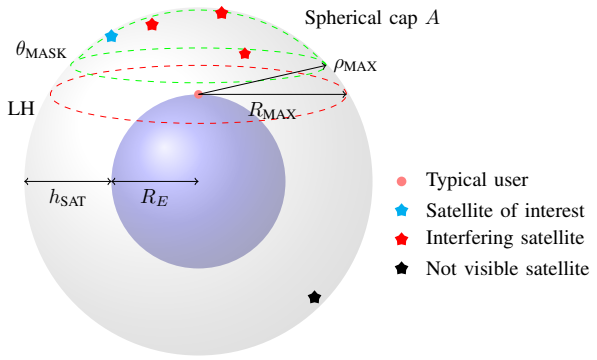

Fig. 3: A typical satellite user view, where the maximum slant range is defined by R_{MAX} at an elevation angle of $0°$. It also shows the usable area as a spherical cap A in green, defined by the minimum elevation angle θ_{MASK}. At the elevation angle θ_{MASK}, the satellite is at the maximum usable distance ρ_{MAX}. The figure also displays different satellites: one of interest, three that could interfere with the satellite of interest, and one out of sight of the user.

in Figure 3. This distance is essential for closing the link budget.

Figure 3 shows a typical satellite user view, where the maximum slant range is defined by R_{MAX} at an elevation angle of $0°$. It also shows the usable area as a spherical cap A in green, defined by the minimum elevation angle θ_{MASK}. At the elevation angle θ_{MASK}, the satellite is at the maximum usable distance ρ_{MAX}. The figure also displays different satellites: one of interest, three that could interfere with the satellite of interest, and one out of sight of the user. In Figure 3, the elevation angle mask θ_{MASK} delimits the coverage area when the user limits its operation due to link budget constraints. The value of θ_{MASK} is crucial, as it significantly impacts the maximum signal propagation

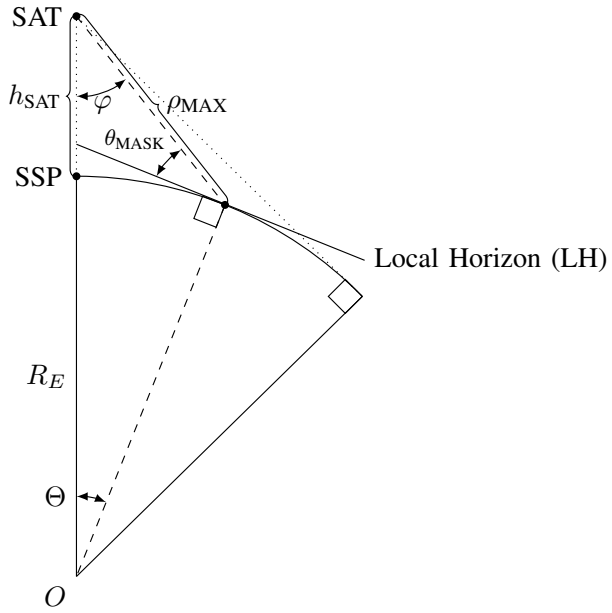

Fig. 4: Distances and angles within a satellite beam depends on the user local horizon (LH), and the altitude of the satellite h_{SAT}.

time between the satellite and the ground station, as well as the maximal losses incurred due to free space path loss (FSPL). This parameter represents the minimum elevation angle required to achieve a certain quality of service, as below this value, the slant range (distance between the user and satellite) is too large, and the channel losses are too high to guarantee the quality of service.

Figure 4 shows a perpendicular cross section of the plane illustrated in Figure 3, aiding in understanding the trigonometric calculations leading to (1). This figure demonstrates the direct relationship between θ_{MASK} and ρ_{MAX} in relation to the altitude of the satellite h_{SAT} plus the radius of the Earth R_{E}.

$$\rho_{\text{MAX}} = (R_E + h_{\text{SAT}}) \frac{\sin\left(\frac{\pi}{2} - \Psi\right)}{\sin\left(\frac{\pi}{2} + \theta_{\text{MASK}}\right)}, \tag{1}$$

Here, we define (2) to simplify the mathematical notation of (1), where the value of Ψ is defined as:

$$\Psi = \theta_{\text{MASK}} + \arcsin\left(\frac{R_E \sin\left(\frac{\pi}{2} + \theta_{\text{MASK}}\right)}{R_e + h_{\text{SAT}}}\right), \tag{2}$$

Additionally, the Local Horizon (LH) is the tangential plane to the Earth's surface at the user's location, used to define the parameters of a satellite pass over this user.

Figure 5 presents a three-dimensional representation of a single satellite pass, expanding the concept of the LH from Figure 4. This depiction emphasizes that the LH depends on the geographical coordinates of the user, defined by latitude ϕ, longitude λ, and altitude above mean sea level h. This implies that for a moving user, the LH will change. However, for our analysis, since the user's speed is much smaller than

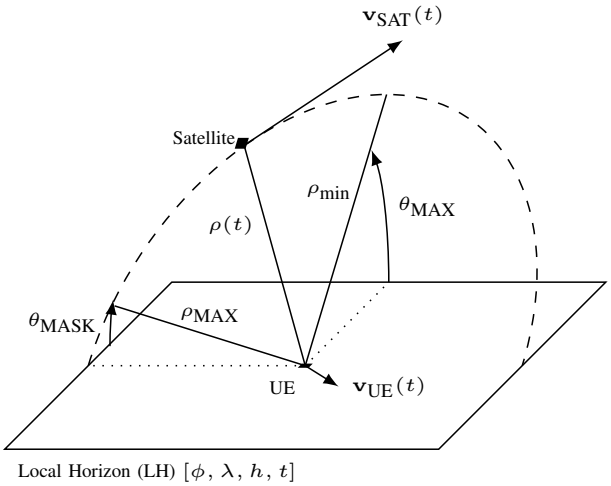

Fig. 5: Parameters involved in a single satellite pass.

the satellite's speed $\mathbf{v}_{\text{UE}}(t) \ll \mathbf{v}_{\text{SAT}}(t)$, we assume the user is static.

Moreover, Figure 5 highlights various parameters that play a critical role in understanding satellite dynamics from the perspective of a ground user, which are integral to the channel model. Among these parameters, θ_{MAX} stands out as particularly significant. It represents the maximum elevation angle that the satellite will attain during a specific pass over the user. This parameter is vital because it influences several other factors, such as the duration of the satellite pass and the minimum distance between the satellite and the user, represented by ρ_{min}. The range of θ_{MAX} is defined as being between $[\theta_{\text{MASK}}, \pi/2]$ if the user's latitude ϕ is smaller than the satellite inclination i, and $[\theta_{\text{MASK}}, \Phi]$ if $\phi > i$, where $\Phi = \pi/2 - \theta_{\text{MASK}} - \phi_{\text{MAX}}$. Here, ϕ_{MAX} is the maximum user latitude where the satellite's maximum elevation angle reaches, at least, the elevation angle mask $\theta_{\text{MAX}} \geq \theta_{\text{MASK}}$. The value of ϕ_{MAX} can be obtained using the law of cosines:

$$\phi_{\text{MAX}} = \arccos\left(\frac{2R_E^2 + h_{\text{SAT}}^2 + 2R_E h_{\text{SAT}} - \rho_{\text{MAX}}^2}{2R_E\left(R_e + h_{\text{SAT}}\right)}\right) \quad (3)$$

It should be noted that each satellite pass will have a unique value of θ_{MAX}, determined by orbital dynamics, the user location, and the time, while:

$$\max\left(\theta_{\text{MAX}}\right) = \begin{cases} \pi/2 & \text{if } i \geq \phi \\ \Phi & \text{if } i < \phi \end{cases} \quad (4)$$

is the maximum value achievable for θ_{MAX}.

Next, we provide a numerical analysis to give the reader a clear understanding of the concepts previously described. Assuming a satellite with $h_{\text{SAT}} = 600$ km, an orbit inclination of $i = 60°$, and an elevation angle mask of $\theta_{\text{MASK}} = 10°$, users within a latitude range of $\phi \in \pm i$ will experience a maximum elevation angle of $\pi/2$ at some point, while users up to latitudes of $\pm 75°$ will be able to close the link budget, as the satellite will reach at least an elevation angle equal to the elevation angle mask at some point. Users above these latitudes and up to $\pm 84°$ will have the satellite in LOS, but it will never exceed θ_{MASK}. Finally, for users located above $\pm 84°$, the satellite will never appear above the horizon. This example only represents the values for the line of sight between the user and satellite and does not take into account any antenna pattern.

From the previous example, there is a time dependency between the user location, the satellite movement, and θ_{MAX}, as both the satellite and Earth move. Stochastic models have been developed in the literature to remove the time dependency, such as the work in [27], where the authors present a statistical model to estimate the elevation angle of a satellite, and the work in [28] presenting a statistical model for the maximum elevation angle of a satellite pass.

For wireless communications, the main parameters of the satellite are the slant range between the i-th satellite and the user, $\rho_i = \|\mathbf{r}_{\text{SATi}} - \mathbf{r}_{\text{UE}}\|$, and the relative speed between the satellite and the user, $\mathbf{v}_{\text{SATi,UE}} = (\mathbf{v}_{\text{SATi}} - \mathbf{v}_{\text{UE}})$. These two parameters determine the delay, path loss, and Doppler shift that the signal will experience at the receiver, as defined by the channel model. To obtain these parameters, there are stochastic models such as those in [29]–[31]. However, those models assume that the number of satellites in view follows a Poisson Point Process, while in our scenario, we assume that there are always 4 satellites in view at random positions on the spherical cap A. This assumption is grounded in projections for future PNT service constellations, which are designed to provide continuous coverage with an average of four satellites visible to users in these regions [32]. The anticipated orbital configurations and satellite densities of these constellations support this level of satellite visibility, making our assumption both feasible and representative for our analysis.

C. Wireless Channel Model

We use a delay/Doppler spread representation of the wireless channel [33], i.e.,

$$\gamma_i(\upsilon, \tau) = \sqrt{L_i}\ h_i \delta(\upsilon - \upsilon_i)\delta(\tau - \tau_i). \quad (5)$$

The channel representation in (5) depends on four parameters: the free space path loss $L_i = \left(\frac{c}{4\pi f_c \rho_i}\right)^2$, a random phase rotation h_i, a delay $\tau_i = \frac{\rho_i}{c}$, and a Doppler shift defined as $\upsilon_i \triangleq -\frac{f_c}{c}\frac{d}{dt}\rho_i$, where $\frac{d}{dt}\rho_i = \hat{\mathbf{u}}_{\text{SATi}}^T \mathbf{v}_{\text{SATi,UE}}$ is the relative speed between the UE and the *i*-th satellite, calculated as the projection of $\mathbf{v}_{\text{SATi,UE}}$ onto $\hat{\mathbf{u}}_{\text{SATi}}$. Then, $\hat{\mathbf{u}}_{\text{SATi}} = \frac{\mathbf{r}_{\text{SATi}} - \mathbf{r}_{\text{UE}}}{\|\mathbf{r}_{\text{SATi}} - \mathbf{r}_{\text{UE}}\|}$ is a unit vector that points from the user to the *i*-th satellite. Finally, h_i represents the initial random phase and is constant for the received signal. Since it is a constant value, it will not affect the correlation process during the acquisition step in the receiver; therefore, we can assume an initial phase of 0.

Furthermore, we assume that the channel is wide-sense stationary (WSS) for the duration of the slot (0.5ms using 30kHz of subcarrier spacing); thus, the values of L_i, τ_i, and υ_i can be considered constant for the duration of the slot.

The mean variation of the delay is on the order of 3ns for 0.5ms of satellite movement, and after one slot, the assumed error is less than 0.001%. This is a realistic assumption that does not compromise the results, as similar NTN models use it [34].

The channel FSPL is modeled by L_i assuming unit gain on both the TX and RX antennas, i.e., omnidirectional. L_i depends on the carrier frequency f_c and ρ_i. A more realistic NTN channel would include other losses, such as tropospheric effects (e.g., gas absorption, rain/cloud attenuation), antenna beam/polarization misalignment, etc. These effects are assumed negligible, as these attenuations are much lower compared to FSPL for transmissions in the L/S frequency bands.

The signal delay τ_i is also considered constant, as the change during a slot is negligible. A more accurate model would include additional ionospheric and tropospheric delays due to signal refraction. These effects have been extensively studied for GNSS receivers and are modeled by the Klobuchar model [35] or the NeQuick model [36], [37]. However, the inclusion of these models could obscure the theoretical analysis of this work, as the model for the interference does not depend on specific values for the effects of satellite dynamics but rather on the differential values of delay and Doppler between satellites, as we will see later.

The model of v shows that the measured Doppler is proportional to the relative speed of the satellite-user link in an ideal scenario, where its value is only affected by the dynamics of the satellite and the user. The channel model in (5) serves as a baseline for the generation of a dataset published in [38]. This dataset includes several user positions, and for each location, several satellite passes are computed with a 1-second resolution. For each pass, the satellite's position and velocity are stored.

III. Transmitted and received signal model

In this section, we present the transmitted signal model and the theoretical framework for analyzing interference between satellites transmitting the PRS.

Our focus is on analyzing the impact of the NTN channel on transmissions from S satellites, assuming LOS conditions and no multipath effects.

A. Downlink Signal Model

The 5G downlink signal model begins with the generation of the PRS sequence for each *i*-th satellite. In 5G NR, the PRS sequence generation follows a mathematical formulation similar to other reference signals in the system, such as the Demodulation Reference Signal (DMRS) and the Channel State Information Reference Signal (CSI-RS). The PRS is generated using a Gold sequence. Below, we describe the Gold sequence generation in detail.

The Gold sequence is a pseudo-random sequence that can be efficiently generated by combining two maximum-length sequences (m-sequences). These m-sequences are produced by Linear Feedback Shift Registers (LFSRs), each defined by a generator polynomial.

A Gold sequence, denoted as $c(n)$, is defined by combining two m-sequences, $x_1(n)$ and $x_2(n)$, as follows:

$$c(n) = x_1(n) \oplus x_2(n + N_c), \tag{6}$$

where:

- $c(n)$ is the Gold sequence.
- $x_1(n)$ and $x_2(n)$ are two m-sequences.
- N_c is a cyclic shift applied to $x_2(n)$ to generate different sequences for different base stations (gNBs) or PRS configurations.
- $\oplus$ denotes bitwise modulo-2 addition (XOR).

Generation of m-sequences $x_1(n)$ and $x_2(n)$:

The m-sequences $x_1(n)$ and $x_2(n)$ are generated using primitive polynomials of degree 31, corresponding to the taps of a 31-stage LFSR. The recursive relations for generating these sequences are:

$$x_1(n + 31) = (x_1(n + 3) \oplus x_1(n)) \text{mod } 2, \tag{7}$$

$$x_2(n{+}31) = (x_2(n{+}3) \oplus x_2(n{+}2) \oplus x_2(n{+}1) \oplus x_2(n)) \text{mod } 2, \tag{8}$$

The choice of these specific feedback taps ensures that the sequences have maximum length and are thus pseudo-random.

The initial states of the m-sequences are crucial for generating different PRS sequences for different base stations. The initial states are determined based on the cell ID ($N_{\text{ID}_{\text{cell}}}$), PRS ID, and other configuration parameters defined in the 3GPP specification.

For $x_1(n)$, the initial state $x_1(0), x_1(1), \ldots, x_1(30)$ is typically set to a predefined value that is not all zeros.

For $x_2(n)$, the initial state $x_2(0), x_2(1), \ldots, x_2(30)$ is a function of the cell ID and PRS configuration, ensuring that each cell can transmit a unique PRS.

The shift N_c is determined by the physical cell ID (PCI) or the PRS occasion index. This ensures that the PRS sequences transmitted by different cells (gNBs) or for different PRS occasions are unique, reducing the likelihood of interference between different PRS signals.

The sequence $c(n)$ is then mapped onto the resource grid (RG) in accordance with 3GPP TS 38.211 Section 7.4.1.7.3 [39] as $\mathbf{A}_i \in \mathbb{C}^{M \times N_{\text{SCS}}}$, where M represents the OFDM symbols and N_{SCS} is the total number of subcarriers of the Resource Grid. The cyclix prefix orthogonal frequency-division modulation (CP-OFDM) modulation is applied by incorporating zero padding prior to the inverse fast Fourier transform (IFFT) operation as per 3GPP TS 38.211 Section 5.3.1 [39]. Following this, the CP is appended by the transmitter. The transmitted signal from satellite i is thus expressed in its complex baseband form, as described by

$$\mathrm{x}_i(t) = \sqrt{P_{\mathrm{TX}}} \sum_{m=0}^{M-1} \sum_{k=0}^{N_{\mathrm{SCS}}-1} A_i[m,k] e^{j2\pi k \Delta f t} \mathrm{rect}\left(\frac{t - mT_s}{T_s}\right), \tag{9}$$

where $T_s = T + T_{\mathrm{CP}}$ indicates the symbol duration as the OFDM symbol time T plus the duration of the CP T_{CP}, $\Delta f = \frac{1}{T}$ is the subcarrier spacing, and $\mathrm{rect}(t/T_s)$ is the rectangular function. We assume the use of the rect pulse as it reduces computational complexity and maintains the orthogonality between subcarriers; therefore, the interference is due to the channel dynamics only.

The transmitted signal $x_i(t)$ has an average power level of P_{TX}. This power level is fixed at the satellite's high power amplifier (HPA) to guarantee minimum performance for beam-edge users. This approach assumes, similar to GNSS, a uniform equivalent isotropic radiated power (EIRP) across the satellite beam.

B. Received Signal Model

The channel model outlined in (5) describes a channel between the *i*-th satellite gNB and the UE. In a positioning system, the user typically receives all downlink signals within the same BWPP spectrum. Thus, the received signal model is an aggregation of different NTN signals, each affected by a distinct channel γ_i. The received signal is modeled by

$$y(t) = \sqrt{L_i} \sum_{i=0}^{\mathrm{S}-1} e^{j2\pi \upsilon_i t + \varrho} x_i(t - \rho_i/c) + w(t), \tag{10}$$

as the aggregation of the signal received by the S satellites in LOS. The model (10) is essential for subsequent analyses, including SINR evaluations and performance assessments of the delay estimator.

C. Matched filter

In the receiver architecture, the matched filter operation is based on the cross ambiguity function (CAF). This process involves correlating the received signal $y(t)$ with the different pilot signals shifted in frequency by a certain known value, analogous to the procedure employed by a GNSS receiver in its acquisition phase. The definition

$$\chi_{xy}(\upsilon, \tau) = \int_{-\infty}^{+\infty} x(t) y^*(t - \tau) e^{j2\pi \upsilon t} dt, \tag{11}$$

illustrates the principle of detector operation, where the received signal is compared against the different local copies of the PRS, one per satellite. Therefore, the receiver will perform at least four different CAF computations.

Substituting the received signal $y(t)$ into the CAF, and following a similar analysis as done in [40], the matched filter output for the *i*-th PRS is given by

$$\begin{aligned}\chi_{yx}^{(i)}(\upsilon, \tau) =& \sqrt{L_i} e^{j2\pi(\upsilon - \upsilon_i)\tau_i} \chi_{xx}^{(i)}(\upsilon - \upsilon_i, \tau - \tau_i) \\ &+ \sum_{\substack{s=0 \\ s \neq i}}^{\mathrm{S}-1} \sqrt{L_s} e^{j2\pi(\upsilon - \upsilon_s)\tau_s} \chi_{x_s x}^{(i)}(\upsilon - \upsilon_s, \tau - \tau_s) \\ &+ \chi_{wx}^{(i)}(\upsilon, \tau).\end{aligned} \tag{12}$$

D. Post-matched filter Signal-to-Noise Plus Interference Ratio Analysis

This subsection concludes the modeling discussion by presenting SINR as a critical key performance indicator (KPI) for analyzing receiver performance. Assessing SINR is paramount for the effective detection of the peak in the receiver's detector.

We know that the maximum value of the ambiguity function (AF) is at the origin $\tau = 0, \upsilon = 0$. By applying a variable change in (12) as $\tau' = \tau - \tau_i$ and $\upsilon' = \upsilon - \upsilon_i$, we shift the origin to the peak, then evaluate the CAF in relation to the difference in delay and Doppler of interference signals. For this, we apply the following change of variables in (12): $\Delta\tau_s = \tau_i - \tau_s$ and $\Delta\upsilon_s = \upsilon_i - \upsilon_s$, yielding

$$\begin{aligned}\chi_{yx}^{(i)}(\tau', \upsilon') &= \sqrt{L_i} e^{j2\pi\upsilon'\tau_i} \chi_{xx}^{(i)}(\upsilon', \tau') \\ &+ \sum_{\substack{s=0 \\ s \neq i}}^{S-1} \sqrt{L_s} e^{j2\pi\left(\upsilon' - \Delta\upsilon_s\right)\tau_s} \chi_{x_s x}^{(i)}(\upsilon' - \Delta\upsilon_s, \tau' - \Delta\tau_s) \\ &+ \chi_{wx}^{(i)}(\upsilon', \tau').\end{aligned} \tag{13}$$

Therefore, we can find the contribution to the signal to noise ratio (SNR) of the signal of interest i from the other s satellites. As mentioned above, the peak of the displaced CAF corresponds to $\upsilon' = 0$ and $\tau' = 0$. Therefore, we define the SINR by setting $\upsilon' = 0$ and $\tau' = 0$ in the CAF:

$$\mathrm{SINR}_i = \frac{L_i P_{\mathrm{TX}}}{\sum_{s \neq i}^{S-1} P_{\mathrm{TX}} L_s |\chi_{x_s x}(\Delta\upsilon_s, \Delta\tau_s)|^2 + |\chi_{wx}(\upsilon_i, \tau_i)|^2} \tag{14}$$

$$= \frac{P_{\mathrm{TX}} \rho_i^{-2}}{\sum_{s \neq i}^{S-1} P_{\mathrm{TX}} \rho_s^{-2} |\chi_{x_s x}(\Delta\upsilon_s, \Delta\tau_s)|^2 + \sigma^2}, \tag{15}$$

where we assume the same transmission power across all satellites, denoted as P_{TX}, and the CAF of the receiver noise as $|\chi_{wx}(\upsilon_i, \tau_i)|^2 = \sigma^2$. This simplification incorporates the concept that the noise power is attenuated by the transmitted power normalized by the FSPL at the *i*-th satellite, represented as $P_{\mathrm{TX}} L_i$.

Consequently, the interference contribution of the remaining satellites to the *i*-th satellite SINR depends on the distance ρ_s and the CAF, and is expressed as

$$I_i = P_{\mathrm{TX}} \sum_{s \neq i}^{S-1} \rho_s^{-2} |\chi_{x_s x}(\Delta\tau_s, \Delta\upsilon_s)|^2. \tag{16}$$

This assumption is valid under the approximation that all satellites transmit at the same wavelength, which is

the characteristic scenario when using a common BWP for transmitting the PRS. Moreover, interference is further influenced by the values of the CAF for the differential delay, denoted as $\Delta\tau_s$, and the differential Doppler shift, represented as $\Delta\upsilon_s$, between the satellite of interest i and the interfering satellite s.

Satellite positions are required to compute their distance to the user, ρ_s. However, a closed form for ρ_s is complex and has several dependencies, such as the time of observation, the position of the user on Earth, the satellite constellation design, the orbit model, etc. From Figure 3, we can see that all satellites are located on a spherical cap, called A. The satellites' azimuth and elevation angles can be considered as uniform random variables, where the azimuth angle is between $[0, 2\pi]$ and the elevation is between $[\theta_{\text{MASK}}, \pi/2]$. However, the distance to the user is not random, as it depends on the azimuth, elevation, and the spherical cap where the satellites lie.

Therefore, to evaluate the interference, a statistical approach is taken. We are interested in the extreme (maximum) values of the interference, as they have a very high impact on receiver performance. In extreme value theory, there are two fundamental approaches, both widely used: the block maxima (BM) method and the peaks-over-threshold (POT) method.

The BM approach consists of dividing the observation period into non-overlapping periods of equal size and focuses on the maximum observation in each period. This approach fits our analysis, as each block can be seen as an OFDM symbol, and we evaluate the maximum value of the interference per symbol.

We use the Fisher–Tippett–Gnedenko theorem, which establishes that the distribution of the maximum value of the BM converges to the Generalized extreme value (GEV) defined in (17).

$$F_{\text{Interference}}(x) = \exp\left(-\left[1 + k\left(\frac{x-\mu}{\sigma}\right)\right]^{-1/k}\right). \quad (17)$$

This GEV distribution is defined by three parameters: k (shape), σ (scale), and μ (location). However, obtaining a closed-form expression for these parameters based on the PRS configuration is not feasible analytically; for this reason, we follow an empirical approach to estimate these parameters. In the next section, we extract the different expressions to model the interference based on the PRS configuration.

IV. Empirical Interference model extraction

This section describes the Monte Carlo simulator developed, the methodology used to extract the interference model empirically, and the parameter models based on the PRS waveform configuration.

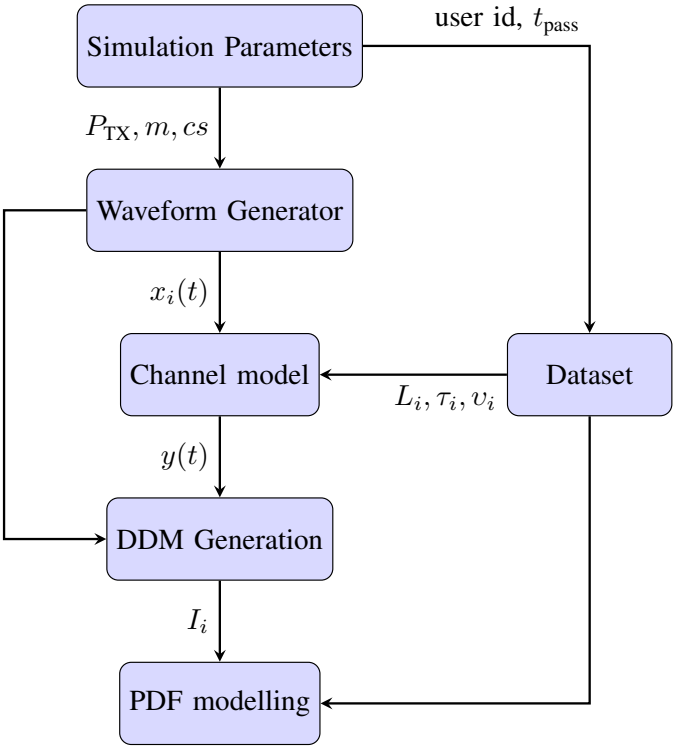

Fig. 6: 5G PRS LEO simulator architecture.

A. Monte Carlo simulator architecture

Figure 6 shows the simulator developed to extract the model for the probability density function (PDF) of the interference as seen in equation (16). This simulator follows a Monte Carlo technique, evaluating the system for different user locations and signal configurations from the public dataset [38] and from a constellation proposed in [32] for the future LEO-PNT mission by ESA. The constellation proposed for this mission consists of 11 orbital planes, with 19 satellites per plane, evenly distributed using polar orbits at an altitude of 1200 km. We will then compare the interference model from both constellations and find a common model that generalizes it to be independent of the constellation design.

The assumption made for the simulator is that all satellites are synchronized and transmit the PRS at the same time but in a different RG arrangement, as shown previously in Figure 2.

The simulator starts with the definition of the simulation parameters, such as the signal configuration and the dataset [38] for the satellite passes. Then, it generates the requested waveforms. The next step is to apply the corresponding channel to each waveform i, where the delay τ_i, losses L_i, and Doppler υ_i are tightly coupled due to satellite movement. The simulator then performs the signal acquisition by computing the DDM of the received signal, composed of the signal of interest and the other interference signals plus noise. Finally, from the DDM, the simulator generates the

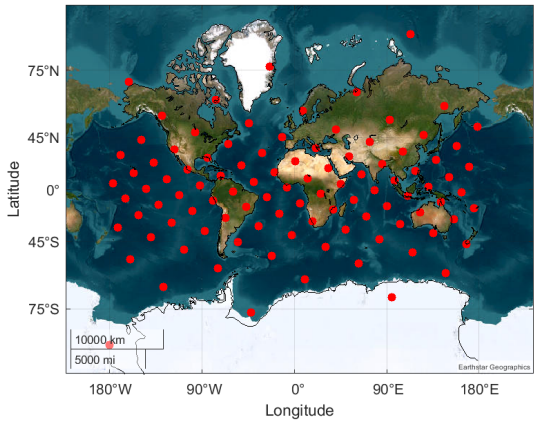

Fig. 7: User's distribution of the dataset.

interference power samples used to analyze its probabilistic behavior.

Both datasets used contain 100 users uniformly spread across Earth's surface (using a Fibonacci lattice). For each user location, 10 minutes of satellite passes are stored with a 1-second resolution. Figure 7 shows the locations of the users on Earth from the dataset used to compute the satellite passes.

The Monte Carlo simulator performs 10,000 iterations per user location and transmitted waveform parameters (number of symbols, Comb Size, and transmitted power). To compute the interference, we follow the procedure illustrated in Figure 6. For each user in the dataset, we generate the transmitted signal and apply a channel model at a randomly selected time, thereby assigning specific values of slant range and velocity to the satellites. After applying the channel model, the acquisition process begins. This process is analogous to the acquisition step in GNSS receivers, wherein a bank of correlators processes the signal using local replicas. A threshold is then applied to ascertain the presence of the signal of interest. If the signal is not detected, the process is repeated with different local replicas. If the signal is detected, we use the simulation environment to evaluate the power of the signal of interest and the power of other signals, which are treated as interference. The obtained interference power values are then used to develop the interference model.

Table I enumerates the parameters relevant to the scenario described in Section II. In this scenario, the number of concurrent satellites in LOS is set to four, which represents the minimum required for 3D position estimation. The bandwidth is set to the minimum permissible for the transmission of the PRS. Similarly, the carrier frequency is chosen as the highest allowed within the n256 band.

Table II shows the various parameter values used to generate the PRS in the simulation. We made a comparison using different numbers of OFDM symbols, various Comb Size values, and different transmission powers.

Table I: Scenario details

Description	Symbol	Value
Number of satellite in LOS	S	4
Maximum signal bandwidth	BW_{MAX}	8.64 MHz
Satellite's constellation 1	Starlink	Inclination of 53 deg/554km
Satellite's constellation 2	LEO-PNT	Polar. 11x19 1200 km
Carrier frequency	f_c	n256 (2.2 GHz)
Number of MC iterations	N_{index}	10000
Doppler Max value	$\pm v_{\text{MAX}}$	40 kHz
Doppler resolution	v_{step}	500 Hz

Table II: PRS generation details.

Description	Symbol	Value
Number of Symbols	m	1 to 12
Number of Subcarriers	N_{SC}	288
Subcarrier Spacing	Δf	30 kHz
Comb Size	cs	4, 6 and 12
Transmitted power	P_{TX}	1 to 30 dBW

B. Distribution parameters extraction for the interference model

As seen in Section III, the statistical interference model in (16) used in the SINR analysis can be modeled by a GEV. However, an analytical evaluation of the GEV parameters μ, σ, k is not feasible in this satellite scenario. Therefore, we present the methodology for using the Monte Carlo approach to extract the distribution parameters of the interference created by the PRS.

Table III shows the KS fitness test and p-value for the different commonly known distributions used to compare the fitness. As predicted by the Extreme Value Theorem seen in Section III, the distribution that best fits the measurements corresponds to the GEV distribution, which has the lowest KS statistic of 0.0142 and the highest p-value of 0.3688.

Furthermore, Figure 8 shows, in discrete blue, the empirical PDF for two different waveform configurations (using 1 and 12 OFDM symbols) from the simulator and, in continuous red, the fitted PDF using a GEV model.

Table III: Kolmogorov-Smirnov test (KS) test and p-test result for the different distribution evaluated.

Distribution	KS	p-test
Normal	0.0382	0
LogNormal	0.0256	0
Gamma	0.0298	0
Rayleigh	0.5295	0
Rician	0.0382	0
GEV	0.0142	0.368

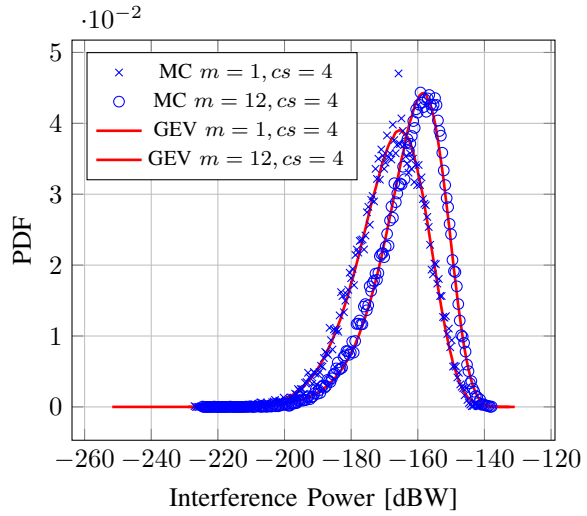

Fig. 8: An example of a PDF of the interference power used to compare the results from the Monte Carlo simulation and the GEV distribution.

Once we evaluated the model that best fits the maximum values of interference, we identified the relationship between the waveform parameters—number of symbols m, Comb Size cs, and transmission power P_{TX}—and the distribution parameters—shape k, scale σ, and location μ. A compromise was found between the complexity of the model and the fitness of the data.

- Scale:
$$\sigma(m) = a_1 + a_2 m + a_3 m^2 \tag{18}$$
- Location:
$$\mu(m, P_{\text{TX}}) = b_1 + b_2 P_{\text{TX}} + b_3 m^{-1/2} + b_4 m P_{\text{TX}} \tag{19}$$
- Shape:
$$k(m) = c_1 + c_2 m^{-1/2} + c_3 m \tag{20}$$

We follow a curve fitting process to obtain the parameters of (18), (19) and (20) using the Levenberg-Marquardt algorithm for least squares minimization. The following table IV shows the numerical values of the parameters for both constellations and a third scenario called "Generic", where we fit the parameters from both scenarios to make the model agnostic of the scenario. Besides, we have added the fitting error as R^2 for each parameter. Furthermore, we also show the residuals between the "Generic" constellation values and the other two to show that this generic model can be used for any constellation design, having into account the error we get. This is a trade off between the complexity of the model and accuracy of it.

The results from Table IV show that the parameter $k < 0$, indicating that the GEV is a bounded distribution (Weibull), suggesting a natural upper limit to interference power. This natural upper limit arises from the output of the DDM when comparing two different signals. Furthermore, the low values of k suggest a low risk of extreme interference power.

Figures 9, 10, and 11 show the models used for the parameters k, σ, and μ using data from the LEO-PNT, Starlink, or both. They also include the 95% confidence interval for the model of both constellations.

- LEO-PNT Model: The R^2 value is higher for all parameters in the LEO-PNT model when applied to its own dataset.
- Starlink Model: The Starlink model has a lower R^2 than the combined model, indicating that the combined model is able to generalize better than the Starlink-specific model in this case.
- Combined Model: The combined model, which fits both the LEO-PNT and Starlink data, has a lower error than the Starlink-specific model, particularly for the parameter μ. This suggests that the combined model provides a good balance in fitting both datasets, sometimes even outperforming one of the specific models (Starlink, in this case).

The combined model benefits from exposure to both datasets, allowing it to find patterns that generalize well across different scenarios, while the Starlink-specific model may overfit to the nuances of the Starlink data, leading to a lower R^2. This explains why the combined model can outperform a model fitted on just one dataset. The combined model generalizes well, making it a robust choice across both datasets.

This model extraction can be used in future designs to evaluate the interference power that a PRS pilot will generate in a typical scenario with reception from four satellites. It can be used to calculate the exceedance probability that the interference power exceeds a certain threshold x, as shown in (21).

$$P(M > x) = 1 - F_{\text{GEV}}(x). \tag{21}$$

By formulating the interference power, we can:

- Quantify Extreme Events: Provide mathematical expressions for the probability and magnitude of extreme interference events.
- Inform Decision-Making: Aid in the design of satellite communication systems that can withstand rare but severe interference events.
- Enhance Reliability: Improve overall performance and reliability by proactively managing the risks associated with extreme interference.

V. Conclusions and Prospects for Future Research

This study presents a model of the interference power in an NTN scenario when using the PRS as a signal for positioning. The model has been extracted empirically using a Monte Carlo approach, as the dynamics of the LEO scenario make it unfeasible to derive a direct mathematical formulation for interference modeling.

Two analytical tools, the CAF and the DDM, have been used in assessing the interference for a PRS signal. These

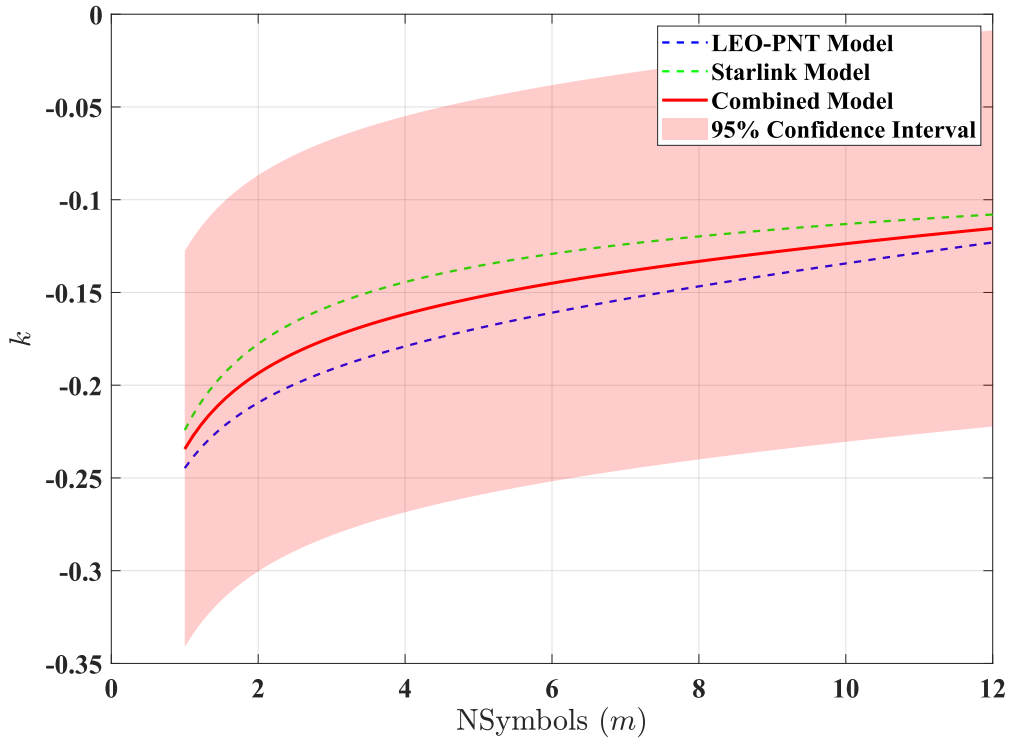

Fig. 9: k value for both dataset separately, k for the combined dataset and the confidence interval

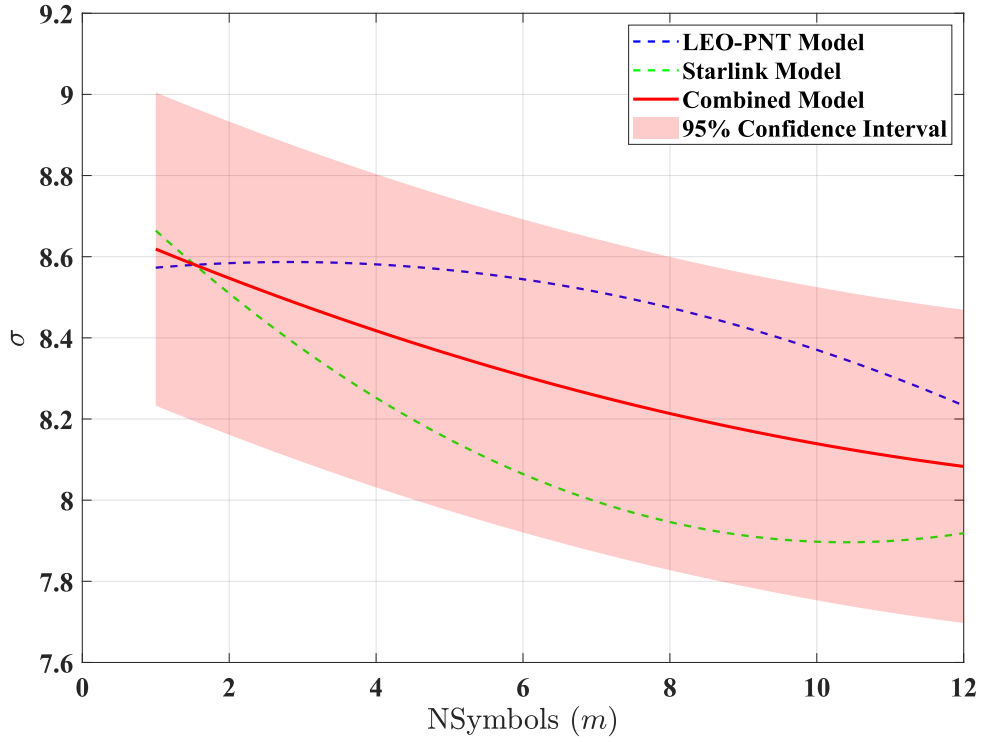

Fig. 10: σ value for both dataset separately, σ for the combined dataset and the confidence interval

Table IV: Comparison of GEV parameters between the Generic, Polar, and starlink scenarios.

Scenario	a_1	a_2	a_3	b_1	b_2	b_3	b_4	c_1	c_2	c_3
LEO-PNT	8.5535	0.0237	-0.0042	199.994	-1.909	8.571	-0.0143	-0.1428	-0.1061	0.0042
Starlink	8.8366	-0.1809	0.0087	195.402	-1.950	13.826	-0.0086	-0.0674	-0.1572	0.0004
Generic	8.6951	-0.0786	0.0023	197.698	-1.929	11.198	-0.0114	-0.1051	-0.1316	0.0023
Residual (LEO-PNT)	0.1416	0.1023	0.0065	2.296	0.020	2.627	0.0029	0.0377	0.0255	0.0019
Residual (Starlink)	0.1415	0.1023	0.0064	2.295	0.021	2.628	0.0028	0.0377	0.0256	0.0019

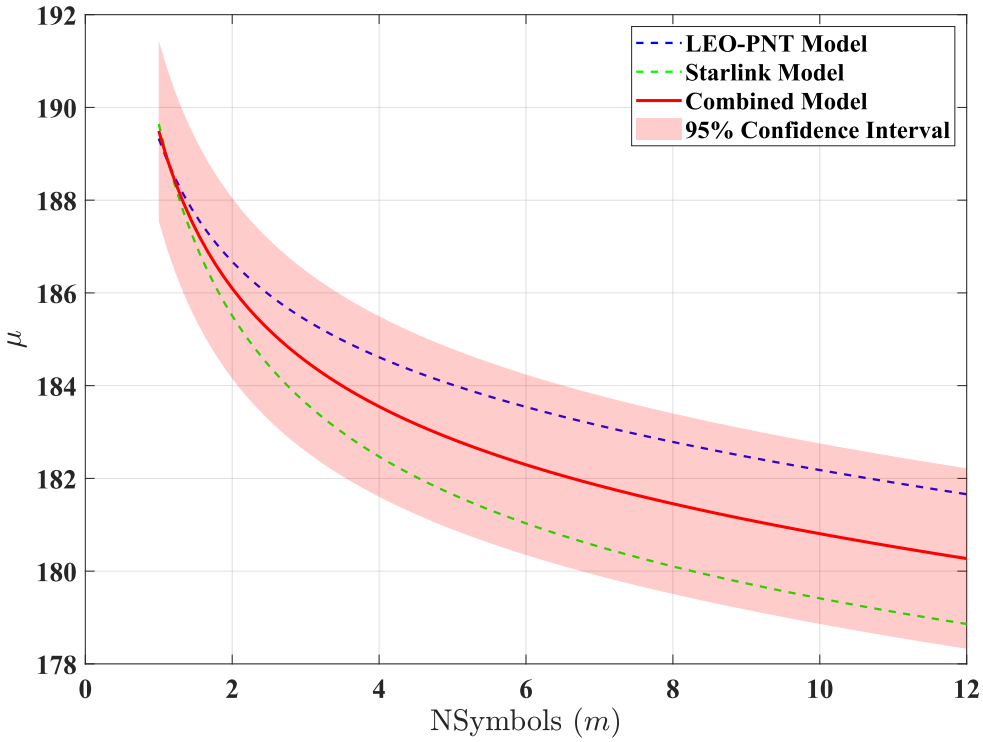

Fig. 11: μ value for both dataset separately, μ for the combined dataset and the confidence interval using $P_{\text{TX}} = 10dBW$

Table V: R^2 metric for the fitting of the curves.

Constellation	R_k^2	R_σ^2	R_μ^2
LEO-PNT	0.91	0.95	0.93
Starlink	0.88	0.92	0.89
Combined	0.90	0.94	0.91

methodologies have paved the way for an open research question: the feasibility of designing a positioning system that multiplexes different transmissions while minimizing interference.

In summary, the findings of this study contribute significantly to the understanding of interference challenges in LEO scenarios and mark a step towards the integration of 5G NTN as an autonomous system, independent of GNSS receivers at the UE end. The results highlight the need for advanced multiplexing strategies to manage multiple satellite signals within the same BWP, thereby mitigating SINR degradation.

Future research includes applying precompensation for delay and Doppler within the beam coverage area, incorporating the ICI and ISI models during DDM computation to reduce their effects, or exploring alternative waveform designs such as orthogonal time frequency space modulation (OTFS), which could leverage their robustness in high Doppler and delay environments. Another avenue for enhancing current results involves implementing a succesive interference cancellation (SIC) algorithm, which holds promise for improving the SINR of the signal [41], or exploiting the sparsity of the DDM matrix by using an orthogonal matching pursuit (OMP) algorithm.

Appendix. Acronyms

This paper uses an extensive number of acronyms, and to assist the reader, the following list presents all of them:

5G	fifth generation
3GPP	3rd Generation Partnership Project
AF	ambiguity function
BWP	bandwidth part
BWPP	bandwidth part for positioning
CAF	cross ambiguity function
CP	cyclix prefix
CP-OFDM	cyclix prefix orthogonal frequency-division modulation
DDM	delay/Doppler map
EIRP	equivalent isotropic radiated power
FFR	fraction frequency reuse
FR1	frequency region 1
FR2	frequency region 2
FSPL	free space path loss
GEV	Generalized extreme value
gNB	next generation base station
GNSS	global navigation satellite system
HAP	high-altitude platform
HPA	high power amplifier
IFFT	inverse fast Fourier transform
IoT	Internet of things
ICI	inter-carrier interference
INI	inter-numerology interference
ISI	inter-symbol interference
KPI	key performance indicator
KS	Kolmogorov-Smirnov test
LEO	low Earth orbit
LOS	line of sight
LTE	Long Term Evolution
NTN	non-terrestrial network
OFDM	orthogonal frequency-division multiplexing
OMP	orthogonal matching pursuit
OTFS	orthogonal time frequency space modulation
PDF	probability density function
PNT	positioning, navigation, and timing
PRS	positioning reference signal
RE	resource element
RG	resource grid
SIB	system information block
SIC	succesive interference cancellation
SINR	signal to interference plus noise ratio
SNO	satellite network operator
SNR	signal to noise ratio
ToA	time of arrival
UAV	unmanned aerial vehicle
UE	user equipment
WSS	wide-sense stationary

Acknowledgement

The simulations presented in this paper were carried out using the HPC facilities of the University of Luxembourg [42] (see `hpc.uni.lu`).

The work presented in this paper was carried out in the framework of SatNEx V WI 3.3: LEO-PNT project, funded by ESA. contract no. 4000130962/20/NL/NL/FE. The authors thank Dr. Nader Alagha from ESA for his constructive discussions. The views expressed in this paper can in no way be taken to reflect the official opinion of the European Space Agency.

References

[1] M. El Jaafari, N. Chuberre, S. Anjuere, and L. Combelles, "Introduction to the 3GPP-defined NTN standard: A comprehensive view on the 3GPP work on NTN," *International Journal of Satellite Communications and Networking*, vol. 41, no. 3, pp. 220–238, 2023, _eprint: https://onlinelibrary.wiley.com/doi/pdf/10.1002/sat.1471. [Online]. Available: https://onlinelibrary.wiley.com/doi/abs/10.1002/sat.1471

[2] C4ADS, "Above Us Only Stars. Exposing GPS Spoofing in Russia and Syria," C4ADS, Tech. Rep., 2019.

[3] A. Grenier, E. S. Lohan, A. Ometov, and J. Nurmi, "A Survey on Low-Power GNSS," *IEEE Communications Surveys & Tutorials*, vol. 25, no. 3, pp. 1482–1509, 2023, conference Name: IEEE Communications Surveys & Tutorials. [Online]. Available: https://ieeexplore.ieee.org/document/10097786

[4] 3GPP, "Study on NR positioning support," 3GPP, Technical Report (TR) 38.855, 2019. [Online]. Available: https://portal.3gpp.org/desktopmodules/Specifications/SpecificationDetails.aspx?specificationId=3501

[5] I. Muursepp, M. Kulmar, O. Elghary, M. M. Alam, T. Chen, S. Horsmanheimo, and J. Scholliers, "Performance Evaluation of 5G-NR Positioning Accuracy Using Time Difference of Arrival Method," in *2021 IEEE International Mediterranean Conference on Communications and Networking (MeditCom)*. Athens, Greece: IEEE, Sep. 2021, pp. 494–499. [Online]. Available: https://ieeexplore.ieee.org/document/9647652/

[6] M. Panchetti, C. Carbonelli, M. Horvat, and M. Luise, "Performance analysis of PRS-based synchronization algorithms for LTE positioning applications," in *2013 10th Workshop on Positioning, Navigation and Communication (WPNC)*. Dresden: IEEE, Mar. 2013, pp. 1–6. [Online]. Available: http://ieeexplore.ieee.org/document/6533292/

[7] F. Rinaldi, H.-L. Maattanen, J. Torsner, S. Pizzi, S. Andreev, A. Iera, Y. Koucheryavy, and G. Araniti, "Non-Terrestrial Networks in 5G & Beyond: A Survey," *IEEE Access*, vol. 8, pp. 165 178–165 200, 2020, conference Name: IEEE Access.

[8] S. E. Trevlakis, A.-A. A. Boulogeorgos, D. Pliatsios, J. Querol, K. Ntontin, P. Sarigiannidis, S. Chatzinotas, and M. Di Renzo, "Localization as a Key Enabler of 6G Wireless Systems: A Comprehensive Survey and an Outlook," *IEEE Open Journal of the Communications Society*, vol. 4, pp. 2733–2801, 2023, conference Name: IEEE Open Journal of the Communications Society. [Online]. Available: https://ieeexplore.ieee.org/document/10287134/references#references

[9] H. K. Dureppagari, C. Saha, H. S. Dhillon, and R. M. Buehrer, "NTN-Based 6G Localization: Vision, Role of LEOs, and Open Problems," *IEEE Wireless Communications*, vol. 30, no. 6, pp. 44–51, Dec. 2023, conference Name: IEEE Wireless Communications. [Online]. Available: https://ieeexplore.ieee.org/document/10355106

[10] Z. Wei, Y. Wang, L. Ma, S. Yang, Z. Feng, C. Pan, Q. Zhang, Y. Wang, H. Wu, and P. Zhang, "5G PRS-Based Sensing: A Sensing Reference Signal Approach for Joint Sensing and Communication System," *IEEE Transactions on Vehicular Technology*, vol. 72, no. 3, pp. 3250–3263, Mar. 2023, conference Name: IEEE Transactions on Vehicular Technology.

[11] N. S. Miller, J. T. Koza, S. C. Morgan, S. M. Martin, A. Neish, R. Grayson, and T. Reid, "SNAP: A Xona Space Systems and GPS Software-Defined Receiver," in *2023 IEEE/ION Position, Location and Navigation Symposium (PLANS)*. Monterey, CA, USA: IEEE, Apr. 2023, pp. 897–904. [Online]. Available: https://ieeexplore.ieee.org/document/10139956/

[12] L. Ries, M. C. Limon, F.-C. Grec, M. Anghileri, R. Prieto-Cerdeira, F. Abel, J. Miguez, J. V. Perello-Gisbert, S. D'Addio, R. Ioannidis, A. Ostillio, M. Rapisarda, R. Sarnadas, and P. Testani, "LEO-PNT for Augmenting Europe's Space-based PNT Capabilities," in *2023 IEEE/ION Position, Location and Navigation Symposium (PLANS)*,

Apr. 2023, pp. 329–337, iSSN: 2153-3598. [Online]. Available: https://ieeexplore.ieee.org/document/10139999/

[13] W. A. Martins, F. Cruz–Roldán, M. Moonen, and P. S. Ramirez Diniz, "Intersymbol and Intercarrier Interference in OFDM Transmissions Through Highly Dispersive Channels," in *2019 27th European Signal Processing Conference (EUSIPCO)*, Sep. 2019, pp. 1–5, iSSN: 2076-1465.

[14] F. Cruz-Roldán, W. A. Martins, F. G. G., M. Moonen, and P. S. R. Diniz, "Intersymbol and Intercarrier Interference in OFDM Systems: Unified Formulation and Analysis," Dec. 2020, arXiv:2012.04527 [eess]. [Online]. Available: http://arxiv.org/abs/2012.04527

[15] M. Nemati and H. Arslan, "Low ICI Symbol Boundary Alignment for 5G Numerology Design," *IEEE Access*, vol. 6, pp. 2356–2366, 2018, conference Name: IEEE Access.

[16] L. Marijanović, S. Schwarz, and M. Rupp, "Multiplexing Services in 5G and Beyond: Optimal Resource Allocation Based on Mixed Numerology and Mini-Slots," *IEEE Access*, vol. 8, pp. 209 537–209 555, 2020, conference Name: IEEE Access.

[17] A. B. Kihero, M. S. J. Solaija, and H. Arslan, "Inter-Numerology Interference for Beyond 5G," *IEEE Access*, vol. 7, pp. 146 512–146 523, 2019. [Online]. Available: https://ieeexplore.ieee.org/document/8861343/

[18] S. A. Khan, A. Kavak, s. Aldirmaz Çolak, and K. Küçük, "A Novel Fractional Frequency Reuse Scheme for Interference Management in LTE-A HetNets," *IEEE Access*, vol. 7, pp. 109 662–109 672, 2019, conference Name: IEEE Access. [Online]. Available: https://ieeexplore.ieee.org/document/8790698

[19] S. Venkatesan, A. Lozano, and R. Valenzuela, "Network MIMO: Overcoming Intercell Interference in Indoor Wireless Systems," in *2007 Conference Record of the Forty-First Asilomar Conference on Signals, Systems and Computers*, Nov. 2007, pp. 83–87, iSSN: 1058-6393. [Online]. Available: https://ieeexplore.ieee.org/document/4487170

[20] N. Trabelsi, L. C. Fourati, and C. S. Chen, "Interference Management in 5G and Beyond Networks," Jan. 2024, arXiv:2401.01608 [cs, eess, math]. [Online]. Available: http://arxiv.org/abs/2401.01608

[21] L. Zhen, A. K. Bashir, K. Yu, Y. D. Al-Otaibi, C. H. Foh, and P. Xiao, "Energy-Efficient Random Access for LEO Satellite-Assisted 6G Internet of Remote Things," *IEEE Internet of Things Journal*, vol. 8, no. 7, pp. 5114–5128, Apr. 2021, conference Name: IEEE Internet of Things Journal. [Online]. Available: https://ieeexplore.ieee.org/document/9222142

[22] X. Lin, J. Bergman, F. Gunnarsson, O. Liberg, S. M. Razavi, H. S. Razaghi, H. Rydn, and Y. Sui, "Positioning for the Internet of Things: A 3GPP Perspective," *IEEE Communications Magazine*, vol. 55, no. 12, pp. 179–185, Dec. 2017, conference Name: IEEE Communications Magazine. [Online]. Available: https://ieeexplore.ieee.org/document/8030544

[23] W. Sixin, T. Xiaomei, L. Xiaohui, F. Wang, and Z. Zhuang, "Doppler frequency-code phase division multiple access technique for LEO navigation signals," *GPS Solutions*, vol. 26, no. 3, p. 98, Jun. 2022. [Online]. Available: https://doi.org/10.1007/s10291-022-01283-7

[24] S. Dwivedi, R. Shreevastav, F. Munier, J. Nygren, I. Siomina, Y. Lyazidi, D. Shrestha, G. Lindmark, P. Ernstrom, E. Stare, S. M. Razavi, S. Muruganathan, G. Masini, A. Busin, and F. Gunnarsson, "Positioning in 5G Networks," *IEEE Communications Magazine*, vol. 59, no. 11, pp. 38–44, Nov. 2021, conference Name: IEEE Communications Magazine. [Online]. Available: https://ieeexplore.ieee.org/document/9665436

[25] F. S. Prol, R. M. Ferre, Z. Saleem, P. Valisuo, C. Pinell, E. S. Lohan, M. Elsanhoury, M. Elmusrati, S. Islam, K. Celikbilek, K. Selvan, J. Yliaho, K. Rutledge, A. Ojala, L. Ferranti, J. Praks, M. Z. H. Bhuiyan, S. Kaasalainen, and H. Kuusniemi, "Position, Navigation, and Timing (PNT) Through Low Earth Orbit (LEO) Satellites: A Survey on Current Status, Challenges, and Opportunities," *IEEE Access*, vol. 10, pp. 83 971–84 002, 2022. [Online]. Available: https://ieeexplore.ieee.org/document/9840374/

[26] P. J. Honnaiah, E. Lagunas, S. Chatzinotas, and J. Krause, "Demand-Driven Beam Densification in Multibeam Satellite Communication Systems," *IEEE Transactions on Aerospace and Electronic Systems*, vol. 59, no. 5, pp. 6534–6554, Oct. 2023, conference Name: IEEE Transactions on Aerospace and Electronic Systems. [Online]. Available: https://ieeexplore.ieee.org/document/10130323

[27] J. M. Gongora-Torres, C. Vargas-Rosales, A. Aragón-Zavala, and R. Villalpando-Hernandez, "Elevation Angle Characterization for LEO Satellites: First and Second Order Statistics," *Applied Sciences*, vol. 13, no. 7, p. 4405, Jan. 2023, number: 7 Publisher: Multidisciplinary Digital Publishing Institute. [Online]. Available: https://www.mdpi.com/2076-3417/13/7/4405

[28] S.-Y. Li and K.-Y. Wang, "Application of maximum elevation angle probability density function to macroscopic selection diversity in low earth orbiting satellite constellation systems," *International Journal of Satellite Communications and Networking*, vol. 30, no. 5, pp. 212–220, 2012, _eprint: https://onlinelibrary.wiley.com/doi/pdf/10.1002/sat.1013. [Online]. Available: https://onlinelibrary.wiley.com/doi/abs/10.1002/sat.1013

[29] A. Talgat, M. A. Kishk, and M.-S. Alouini, "Stochastic Geometry-Based Analysis of LEO Satellite Communication Systems," *IEEE Communications Letters*, vol. 25, no. 8, pp. 2458–2462, Aug. 2021, conference Name: IEEE Communications Letters. [Online]. Available: https://ieeexplore.ieee.org/document/9218989

[30] N. Okati, T. Riihonen, D. Korpi, I. Angervuori, and R. Wichman, "Downlink Coverage and Rate Analysis of Low Earth Orbit Satellite Constellations Using Stochastic Geometry," *IEEE Transactions on Communications*, vol. 68, no. 8, pp. 5120–5134, Aug. 2020, conference Name: IEEE Transactions on Communications.

[31] T. A. Khan and M. Afshang, "A Stochastic Geometry Approach to Doppler Characterization in a LEO Satellite Network," in *ICC 2020 - 2020 IEEE International Conference on Communications (ICC)*, Jun. 2020, pp. 1–6, iSSN: 1938-1883. [Online]. Available: https://ieeexplore.ieee.org/document/9148880

[32] A. González, Tobías, I. Rodriguez, P. Navarro, F. Sobrero, E. Carbonell, D. Calle, and J. Fernández, "LEO Satellites for PNT, the Next Step for Precise Positioning Applications," in *Proceedings of the 35th International Technical Meeting of the Satellite Division of The Institute of Navigation (ION GNSS+ 2022)*, Sep. 2022, pp. 2573–2581, iSSN: 2331-5954. [Online]. Available: http://www.ion.org/publications/abstract.cfm?jp=p&articleID=18436

[33] Y. Hong, T. Thaj, and E. Viterbo, *Delay-Doppler communications principles and applications*. London: Academic Press, an imprint of Elsevier, 2022, oCLC: 1297827135.

[34] V. M. Baeza, E. Lagunas, H. Al-Hraishawi, and S. Chatzinotas, "An Overview of Channel Models for NGSO Satellites," in *2022 IEEE 96th Vehicular Technology Conference (VTC2022-Fall)*, Sep. 2022, pp. 1–6, iSSN: 2577-2465. [Online]. Available: https://ieeexplore.ieee.org/document/10012693

[35] J. A. Klobuchar, "Ionospheric Time-Delay Algorithm for Single-Frequency GPS Users," *IEEE Transactions on Aerospace and Electronic Systems*, vol. AES-23, no. 3, pp. 325–331, May 1987, conference Name: IEEE Transactions on Aerospace and Electronic Systems. [Online]. Available: https://ieeexplore.ieee.org/document/4104345

[36] G. Di Giovanni and S. M. Radicella, "An analytical model of the electron density profile in the ionosphere," *Advances in Space Research*, vol. 10, no. 11, pp. 27–30, Jan. 1990. [Online]. Available: https://www.sciencedirect.com/science/article/pii/027311779090301F

[37] J. Sanz Subirana, J. M. Juan Zornoza, and M. Hernández-Pajares, *GNSS DATA Processing. Fundamentals and algorithms. Vol. 1*. Noordwijk: ESA Communications, 2013, oCLC: 922681096.

[38] A. Gonzalez-Garrido, "Starlink satellite passes," 2024, tex.entrytype: data. [Online]. Available: https://dx.doi.org/10.21227/qggt-xr49

[39] 3GPP, "NR; Physical channels and modulation," 3GPP, Technical Specification (TS) 38.211, 2024. [Online]. Available: https://portal.3gpp.org/desktopmodules/Specifications/SpecificationDetails.aspx?specificationId=3213

[40] J. Querol, A. Alonso-Arroyo, R. Onrubia, D. Pascual, H. Park, and A. Camps, "SNR Degradation in GNSS-R Measurements Under the Effects of Radio-Frequency Interference," *IEEE Journal of Selected Topics in Applied Earth Observations and Remote Sensing*, vol. 9, no. 10, pp. 4865–4878, Oct. 2016, conference Name: IEEE Journal of Selected Topics in Applied Earth Observations and Remote Sensing.

[41] N. I. Miridakis and D. D. Vergados, "A Survey on the Successive Interference Cancellation Performance for Single-Antenna and Multiple-Antenna OFDM Systems," *IEEE Communications Surveys & Tutorials*, vol. 15, no. 1, pp. 312–335, 2013, conference Name: IEEE Communications Surveys & Tutorials.

[42] S. Varrette, H. Cartiaux, S. Peter, E. Kieffer, T. Valette, and A. Olloh, "Management of an academic HPC & research computing facility: The ULHPC experience 2.0," in *Proc. of the 6th ACM high performance computing and cluster technologies conf. (HPCCT 2022)*. Fuzhou, China: Association for Computing Machinery (ACM), Jul. 2022.

Alejandro Gonzalez-Garrido PhD student at the SIGCOM group of SnT (University of Luxembourg), specializing in hybrid GNSS and 5G PNT systems using Non-Terrestrial Networks. Holds an integrated degree and an M.Sc. in Telecommunication Engineering, obtained in 2015. Has professional experience in the timing and synchronization industry, satellite design, and network operations.

Jorge Querol received his Ph.D. degree in Telecommunication Engineering from the Polytechnic University of Catalonia (UPC-BarcelonaTech), Barcelona, Spain, in 2018. His research interests include Software-Defined Radios (SDR), real-time signal processing, satellite communications, satellite navigation, and remote sensing. Jorge joined the Signal Processing and Satellite Communications group (SIGCOM), headed by Prof. Bj"orn Ottersten, and he will be working with Dr. Symeon Chatzinotas.

Henk Wymeersch (S'01, M'05, SM'19, F'24) obtained the Ph.D. degree in Electrical Engineering/Applied Sciences in 2005 from Ghent University, Belgium. He is currently a Professor of Communication Systems with the Department of Electrical Engineering at Chalmers University of Technology, Sweden. He is Senior Member of the IEEE Signal Processing Magazine Editorial Board. During 2019-2021, he was an IEEE Distinguished Lecturer with the Vehicular Technology Society. His current research interests include the convergence of communication and sensing, in a 5G and Beyond 5G context.

Symeon Chatzinotas (MEng, MSc, PhD, F.IEEE) is currently Full Professor / Chief Scientist I and Head of the research group SIGCOM in the Interdisciplinary Centre for Security, Reliability and Trust, University of Luxembourg.

In the past, he has lectured as Visiting Professor at the University of Parma, Italy and contributed in numerous R&D projects for the Institute of Informatics & Telecommunications, National Center for Scientific Research "Demokritos" the Institute of Telematics and Informatics, Center of Research and Technology Hellas and Mobile Communications Research Group, Center of Communication Systems Research, University of Surrey. He has received the M.Eng. in Telecommunications from Aristotle University of Thessaloniki, Greece and the M.Sc. and Ph.D. in Electronic Engineering from University of Surrey, UK in 2003, 2006 and 2009 respectively. He has authored more than 700 technical papers in refereed international journals, conferences and scientific books and has received numerous awards and recognitions, including the IEEE Fellowship and an IEEE Distinguished Contributions Award. He is currently in the editorial board of the IEEE Transactions on Communications, IEEE Open Journal of Vehicular Technology and the International Journal of Satellite Communications and Networking.